Applied Geochemistry 145 (2022) 105430

Contents lists available at ScienceDirect

Applied Geochemistry

journal homepage: www.elsevier.com/locate/apgeochem

Soils developed on the Si-poor, alkali-rich pyroclastic rocks of the Colli Albani volcanic district (Central Italy): The effect of leucite, clinopyroxene and phlogopite on the base cations mobility

M. Gaeta [a,*], L. Aldega [a], M.L. Astolfi [b], B. Bonechi [a], F. Marra [c], P. Pacheco [d], C. Perinelli [a,e], F. Tiberi [a]

[a] Dipartimento di Scienze Della Terra, Sapienza Università di Roma, P. le Aldo Moro 5, 00185, Rome, Italy
[b] Dipartimento di Chimica, Sapienza Università di Roma, P. le Aldo Moro 5, 00185, Rome, Italy
[c] Istituto Nazionale di Geofisica e Vulcanologia, Via di Vigna Murata 605, 00143, Rome, Italy
[d] ÔMINA ROMANA, Via Fontana Parata 75, 00049, Velletri, RM, Italy
[e] C.N.R-Istituto di Geologia Ambientale e Geoingegneria C/o Dipartimento di Scienze Della Terra, Sapienza Università di Roma, Italy

ARTICLE INFO

Editorial handling by : Marcello Liotta

Keywords:
Volcanic soils
Clinopyroxene
Gothic texture
Phlogopite
Halloysite
Colli albani

ABSTRACT

The Colli Albani volcanic district emplaced huge pyroclastic-flow deposits up to 20 m thick in the southeastern suburbs of the City of Rome. The soil quality onto the gentle slopes of the Colli Albani has certainly contribute to the growth of Ancient Rome, a city with one million inhabitants as early as 2000 years ago. Interestingly, the Colli Albani soils developed on K-foiditic pyroclastic rocks with peculiar low silica, high alkali and high CaO composition. In the past, the productivity of the Colli Albani soils was maximized without the understanding of the unique physical, chemical, and mineralogical properties of these soils; now an in-depth knowledge of the Colli Albani soils is necessary to respond to the current and increasingly demand of sustainable soil use. Textural, mineralogical and chemical data indicate that the evolutionary stages of soil development are bedrock →leucite (Lct)-bearing soils→quartz (Qz)-bearing soils. The bedrock is made up mainly of leucite, clinopyroxene, phlogopite, zeolites and K-foiditic glass that is turned in an amorphous phase characterized by the Al-rich, cations base-poor and hydrated composition (i.e. halloysite-like chemistry). This reaction occurs in the syndepositional conditions (i.e. temperature up to ~600 °C) and causes the absence of glass and the abundant crystallization of halloysite in the Colli Albani soils. The Lct-bearing soils are organic matter-poor, weakly weathered volcanic matter, comparable to the vitric andosols, showing incipient halloysite crystallization. As the degree of weathering increases, i) grain size decrease, ii) pH remain neutral, iii) highly soluble leucite, analcime and other zeolites, are rapidly dissolved, iv) alkali, Ca and Mg are leached, v) silica, Al and Fe activities increase and vi) halloysite stability field enlarges. The resulting Qz-bearing soils are made up mainly of halloysite, quartz, oxy-phlogopite and calcic clinopyroxene showing a lower cation exchange capacity (CEC) compared to the Lct-bearing soils. However, in Qz-bearing soils the CEC it is rarely <20 cmol (+)kg^{-1} because K_{Ex}, Mg_{Ex} and Ca_{Ex} are released from the oxy-phlogopite and the strongly weathered clinopyroxenes characterized by the "gothic" texture.

1. Introduction

The unique properties of volcanic soils are largely due to the formation of noncrystalline materials (e.g., active Al and Fe– allophane, imogolite, ferrihydrite, Al/Fe–humus complexes) directly related to the weathering of the glassy particles occurring in pyroclastic parent rocks (e.g. Dahlgren et al., 2004). However, the weathering of volcanic glass is a rapid process (i.e. glass half-lives range from 1650 to 7000 years; Kirkman and Mc Hardy, 1980; Ruxton, 1988; Shojiet al., 1993) and the presence of noncrystalline materials cannot be used to explain the properties of soils developed on relative ancient volcanic deposit or the slope of inactive volcanoes. On the other hand, large regions of volcanic soils form, generally, on pyroclastic or basaltic plateaus with at least a Pleistocene age. Generally, the pyroclastic plateaus have high silica and

* Corresponding author.
E-mail address: mario.gaeta@uniroma1.it (M. Gaeta).

https://doi.org/10.1016/j.apgeochem.2022.105430
Received 30 March 2022; Received in revised form 7 August 2022; Accepted 17 August 2022
Available online 22 August 2022

alkali (SiO_2>52 wt%; alkali>5 wt%) and low CaO (<5 wt%) contents while, the basaltic plateaus, have low silica and alkali (SiO_2<52 wt%; alkali<5 wt%) and high CaO (>5 wt%) contents. These volcanic bedrocks also show different density and textures. The pyroclastic bedrocks have low density (1.10–2.30 g/cm^3) and can be loose or consolidated. The basaltic bedrocks have high density (2.75–3.10 g/cm^3) and are commonly welded. Modest volumes of basaltic scoria blankets can represent of loose, low density, low SiO_2 and high CaO volcanic bedrocks but not of the richness in alkali. The Colli Albani volcanic district (hereafter Colli Albani) offers a unique opportunity to study a relatively wide area (>1500 km^2; Freda et al., 1997) of soils developed on pyroclastic rocks, which are characterized by low silica, high alkali and high CaO contents (e.g. Freda et al., 2011). The eruptive history of Colli Albani spans from 608 ka to 36 ka (Gaeta et al., 2016) and emplaced huge (>280 km^3) pyroclastic-flow deposits that mantle the surface with a volcanic cover. This cover spreads, radially, as far as 50 km from the vent (e.g. Marra et al., 2019), reaching the southeastern suburbs of the City of Rome. This is the most populous and largest (i.e. 1287.36 km^2) municipality in Italy and the third the European Union after Berlin and Madrid. This huge anthropogenic pressure creates the need for extensive knowledge of the Colli Albani volcanic soils that have been developed on a peculiar K-foiditic bedrock (Gaeta et al., 2021). This knowledge is necessary to respond to the increasing demand for sustainable soils use.

In this paper, we provide textural, mineralogical and chemical data for soils in an area of Colli Albani which has been historically dedicated to the *Vitis vinifera* cultivars. Our results provide evidence for soils developed on Si-poor, alkali-rich and CaO-rich pyroclastic rocks in which the typical cation exchange capacity (hereafter CEC) that commonly increases with increasing clay and organic matter content is not observed. Instead, the base cations mobility appears mainly controlled by the dissolution of alkali-rich primary minerals (i.e. leucite, analcime and other zeolites) and exchange reactions with the phlogopite and the calcic clinopyroxene.

2. Study area and soil materials

The study area (i.e. La Parata locality, Fig. 1) is on the south-west slope of the Colli Albani at elevation between 90 and 110 m above sea level and it is characterized by annual average temperatures of 15.5 °C with an average rainfall of around 1000/1200 mm per year, mostly in the autumn and winter. Haplic Phaeozems and Luvic Phaeozems should be the main soils of the study area (1:250000 map of Lazio soils; Napoli et al., 2019) developed on the geologic substrate occurring at 1.5–2.5 m of depth. The bedrock is constituted by depositional units of the Villa Senni eruption (Fig. 1) at 365 ± 4 ka (e.g. Marra et al., 2009; Gaeta et al., 2016). This pyroclastic rock is made up of submillimeter-to decimeter-sized lithic clasts and black to purple scoria clasts enclosed within a crystal-rich matrix. Among the lithic clasts the leucite-bearing granular rocks (i.e. Italites, Gaeta et al., 2000, 2006; Fabbrizio et al., 2018) are particularly abundant. The abundance of Italites, the high phenocrysts content of the scoria clasts and the consolidate matrix indicate that the bedrock is the consolidated facies of the upper flow unit of the Villa Senni eruption known in the literature as Tufo di Villa Senni (e.g. Freda et al., 1997; hereafter TVS). Bedrock bulk composition is phonotephritic to shoshonitic (Fig. 2); on the other hand, vitrophiric scoria clasts, formed at a high cooling rate, are K-foiditic in composition (e.g. Gaeta, 1998).

The field survey of soils was carried out on the basis of the carefully

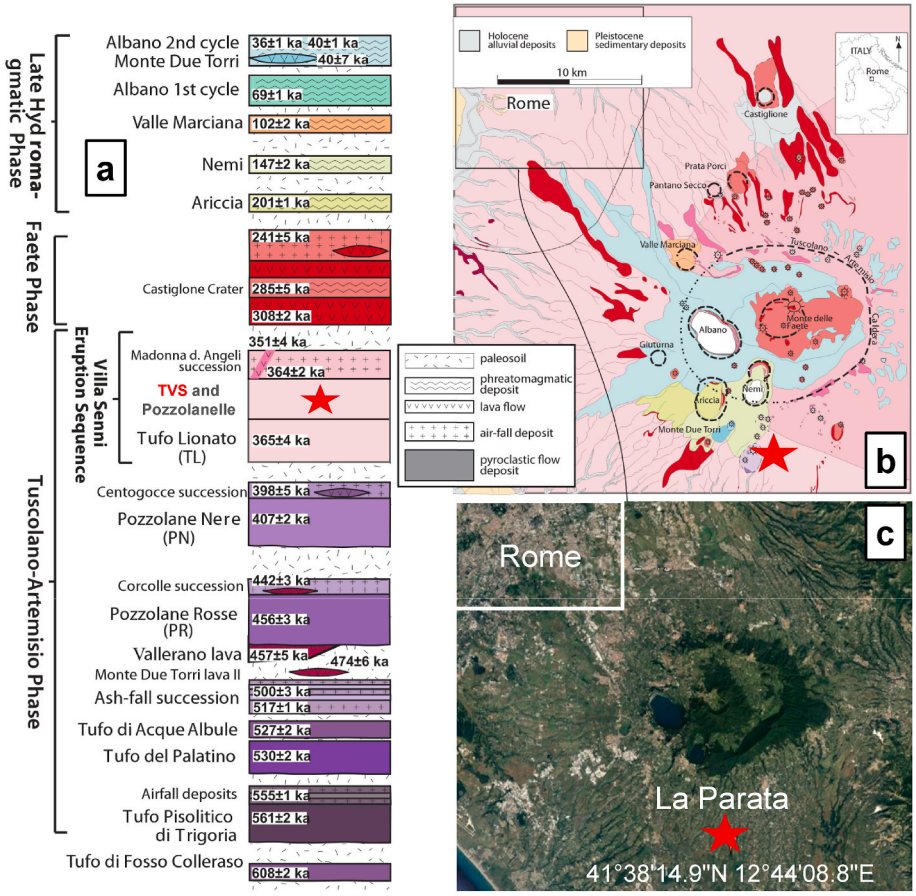

Fig. 1. Stratigraphic successions and chronological constraints available for the Colli Albani Volcanic District (a). Simplified geological map of the Colli Albani Volcanic District with the same colours used in the stratigraphic successions (b). Satellite image showing the geomorphology of the Colli Albani Volcanic District (c). The red star indicates the study area. (For interpretation of the references to colour in this figure legend, the reader is referred to the Web version of this article.)

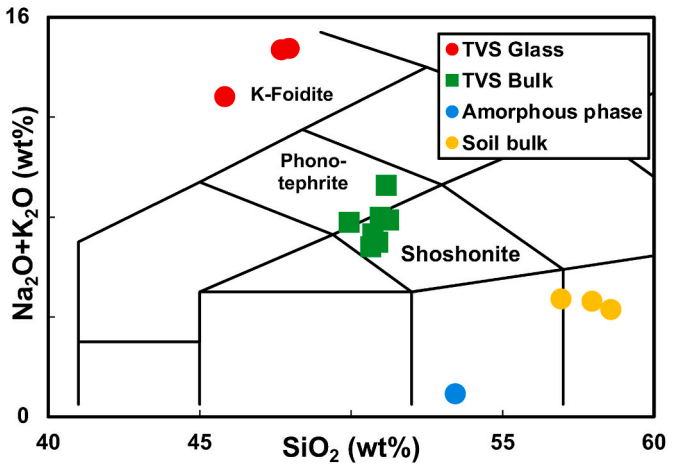

Fig. 2. Bedrock and soil bulk compositions reported in the alkali vs silica classification diagram. Composition of the glass and the amorphous phase occurring in the TVS bedrock are also reported for comparison. Data from Gaeta et al. (2006); Marra et al. (2009); Marra et al. (2011) and Table 1EA.

observation of 13 profiles up to 120 cm of depth (Fig. 3). The profiles show little colour change with depth and indicate the occurrence of two main types of soils: the most diffuse dark to bright brown (10YR3/3,10YR5/8), clayey soils and the gray (10YR6/29), sandy soils (Fig. 3). The clayey soils are enriched of sandy fraction towards the base and occur in the higher topographic zone (i.e. 100-110 m a.s.l.) respect to the sandy soils (i.e. 93-100 m a.s.l.). Vertical transition from the higher clayey soils to the lower sandy soils was clearly individuated in the profile PA6 (Fig. 1 EA). In both groups of soils, the coarse fragments are scarce, and the carbonates are virtually absent while, euhedral to sub-euhedral crystals of clinopyroxene, mica, leucite and analcime, are abundant. This highlights the origin from the underlying volcanic deposit. However, the pedogenetic processes that origin these soils are certainly complex as suggested by the increase of silica content in the soil bulk compositions with respect to those of the bedrock (Fig. 2) that is, typically, quartz-free. Aiming to investigate the pedogenetic processes of Colli Albani soils we sampled the 13 profiles at ~40 cm of depth for the laboratory analyses (Table 1, Fig. 3). This sampling depth, below the manipulated part of the soil and above the bedrock, ensures the representativity of soil samples being the 13 profiles relatively homogeneous.

3. Methods

Physical and chemical analyses were performed for the air-dried fine-earth fraction (<2 mm), according to the procedures outlined by Bozzano et al. (2006) unless otherwise specified. The cation exchange capacity (CEC) was estimated as the ammonium acetate extractable Ca, Mg, K and Na sum. Actually, this method is preferable at the direct measure of CEC in soils without carbonates and with neutral/acid pH (Ross and Ketterings, 1995). Ammonium acetate extraction was performed together that with deionized water. Actually, it is generally recognized that water extraction is considered to be representative of the base cations concentration in the soil solution that, in turn, is representative of mineral-water equilibria. Loss on ignition (LOI) analyses were performed by heating the samples at 105 °C, 550 °C and 950 °C. Total acid digestion of the soil samples was performed in a close microwave oven system (Ethos1 Touch Control; Milestone, Sorisole, Bergamo, Italy). About 0.1 g of soil was mixed with 3 mL HNO_3 69% (superpure; Carlo Erba Reagents, Milan, Italy), 1 mL HF 40% (suprapure; Merck, Darmstadt, Germany), and 1 mL HCl 30% (superpure; Carlo Erba Reagents, Milan, Italy) in a 100 mL polytetrafluoroethylene (PTFE) vessel, and then heated to 180 °C with microwave energy (at a power of 1000 W) for 40 min (Astolfi et al., 2020). At the end, cooled samples were diluted to 10 mL of deionized H_2O (resistivity, ≤18.3 MΩ cm) from an Arioso Power I RO-UP Scholar UV system (Human Corporation, Songpa-Ku, Seoul, Korea) and filtered with syringe filters with cellulose nitrate membranes (GVS Filter Technology, Indianapolis, USA; pore size, 0.45 mm). For the leaching tests, weighed amounts (~0.5 g) of the soil samples were transferred into polypropylene tubes and then brought to a volume of 10 mL with deionized H_2O (W subscript in the text) or 1.0 M solution of CH_3COONH_4 (Ex subscript in the text) (Merck, Darmstadt, Germany). The tubes were then covered with a cap and left under mechanical stirring for 24 h by a rotary shaker (SB2, Cheimika, SA, Italy) at room temperature (21 °C). The extracted solutions were filtered with syringe filters with cellulose nitrate membranes and mixed with 1% HNO_3.

3.1. Elemental analysis

The total and leachable contents of eight elements (Al, Ca, Fe, K, Mg, Mn, Na, and Si) were determined by inductively coupled plasma optical emission spectrometry (ICP-OES; Vista MPX CCD Simultaneous; Varian, Victoria, Mulgrave, Australia) in axial view mode and equipped with inert components (demountable torch with an alumina injector and PTFE injector holder; Sturman-Masters inert spray chamber, double pass, white Ertalyte; Agilent, Santa Clara, CA, United States) for the analysis of digests. Before the ICP-OES analysis, the digests and the extracted solutions "Ex" were diluted 1:10 with 1% HNO_3. The ICP-OES operating parameters were reported elsewhere (Astolfi et al., 2017). Calibration standards of all elements were prepared daily by diluting a single standard solution at 1000 mg/L (Merck, Darmstadt, Germany). Yttrium at 0.5 mg/L (from 1000 ± 2 mg/L; Panreac Química, Barcelona, Spain) was used as an internal standard for all measurements. The

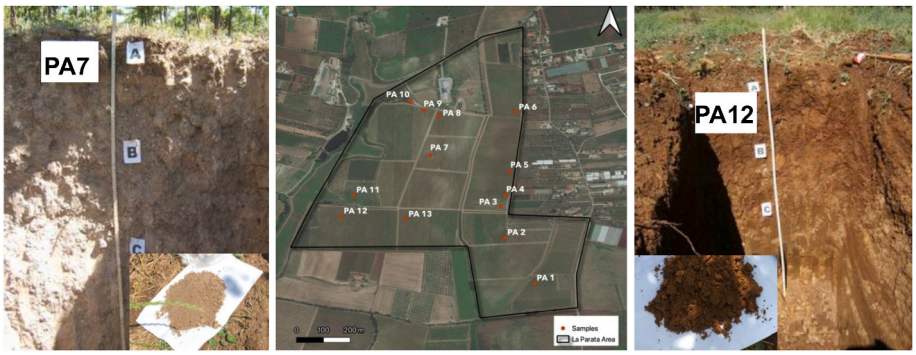

Fig. 3. Profiles and field aspect of the two types of soils in the investigated area. Most diffuse, brown and clayey soils (right) and gray and sandy soils (left) are shown. Location of sampling sites is shown in the photo in the center. Samples for laboratory analyses were collected at about 40 cm of depth. (For interpretation of the references to colour in this figure legend, the reader is referred to the Web version of this article.)

Table 1
Basic properties of the soils.

Sample	Colour	Clay	Silt	Sand	LOI	OM	pH	CEC
		(wt%)						(cmol (+) kg^{-1})
PA3	Gray (10YR6/29)	9	21	70	13.58	1.21	7.6	22.02
PA7		13	13	74	13.65	0.70	7.7	25.11
PA10		13	16	71	14.40	0.92	7.3	23.78
PA11		15	11	74	12.56	0.77	7.0	24.23
PA1	Dark to bright-brown (10YR3/3,10YR5/8)	39	20	41	16.66	1.79	6.8	15.64
PA2		16	15	69	22.96	1.08	7.2	19.32
PA4		28	20	52	18.81	1.28	7.3	21.16
PA5		57	19	24	22.06	1.98	6.3	16.02
PA6		39	18	43	20.75	1.79	6.9	16.14
PA8		45	20	35	22.14	2.30	6.4	17.11
PA9		33	16	51	22.45	0.83	6.5	20.09
PA12		57	16	27	20.31	1.40	6.1	17.39
PA13		49	27	24	22.18	2.55	6.3	16.78

LOI: loss of ignition; OM: organic matter; CEC: cation exchange capacity.

following wavelengths (nm) were used: Al 396.152, Ca 315.887, Fe 238.204, K 766.491, Mg 279.800, Mn 257.610, Na 588.995, Si 251.611, and Y 371.029. The analytical precision (2 sigma error) is between 5 and 10%.

3.2. X-ray diffraction (XRD)

X-ray diffraction analysis of bedrock and soils was conducted using a Bruker D8 Advance X-ray system equipped with Lynxeye XE-T silicon-strip detector at the Department of Earth Sciences, Sapienza University of Rome. The instrument was operated at 40 kV and 30 mA using CuKα radiation (λ = 1.5406 Å). Samples were run between 2 and 70° 2θ with step sizes of 0.02° 2θ while spinning the sample. Data were collected with variable slit mode to keep the irradiated area on the sample surface constant and converted to fixed slit mode to identify whole-powder composition. The relative abundance of minerals was estimated by calculating peak areas and using mineral intensity factors as calibration constants (Moore and Reynolds, 1997).

3.2.1. Scanning electron microscopy and microanalysis

Secondary electron (SE) images used to investigate textural aspects of soils were collected by Scanning Electron Microscopy (SEM) using a FEI-quanta 400 equipped for qualitative microanalysis with an EDAX Genesis system at the Earth Sciences Department, Sapienza University of Rome. Quantitative microanalyses were carried out at the CNR-Istituto di Geologia Ambientale e Geoingegneria di Roma, with a Cameca SX50 electron microprobe equipped with five wavelength dispersive spectrometers (WDS). Analyses were performed using 15 kV accelerating voltage and 15 nA beam current. As standards we employed metals for Mn and Cr, Jadeite for Na, Wollastonite for Si and Ca, Orthoclase for K, Corundum for Al, Magnetite for Fe, Rutile for Ti, Periclase for Mg, Apatite for P. Counting times for all elements were 20 s on peak and 10 s on both backgrounds. Light elements (Na, K) were counted first to prevent loss by volatilization. The PAP correction method was used. Hard minerals (e.g. clinopyroxene) were analyzed using a beam diameter of 1 μm whereas to minimize alkali loss during soft phases (e.g. leucite, zeolites, glass) analysis, the beam was defocused to 15 μm. In order to evaluate the accuracy of the analyses, repeated analyses of three international secondary standards (Kakanui augite, Iceladic Bir-1 and rhyolite RLS132 glasses from USGS) were made prior to any series of measurements. The mean precision from the standard value was about 1% for SiO_2, 2% for Al_2O_3, 5% for K_2O, CaO and FeO, and 8–10% for other elements. The analytical precision (2 sigma error) is 1% for elements in the concentration range >10 wt% oxide, 5% for elements in the range 2–10 wt% oxide and better than 10% for elements in the range 0.5–2 wt.% oxide.

4. Results

4.1. Bedrock texture and mineral chemistry

Scoria clasts in the TVS bedrock are porphyritic (13 vol% in average of phenocrysts) and sparsely vesiculated (Fig. 4). Leucite, clinopyroxene, and phlogopite (Table 1EA), up to millimeter-sized, are ubiquitous phenocrysts and their abundance increases towards the top of the bedrock. Apatite, Fe–Ti-oxides and garnet occur as phenocrysts. The scoria clasts groundmass is made up of a microcrystalline aggregate of clinopyroxene, leucite and zeolites. Rare sanidine xenocrysts are present in the bedrock matrix. The latter is consolidated and made-up of zeolites ± glass (Fig. 4). Larger analyzable zeolites, are, usually, chabazitic in composition (Table 1EA) although phillipsite occurrence is also pointed out by the XRD analysis (Table 2; Fig. 2EA). The matrix glass of the TVS bedrock is turned in an amorphous, pale yellow phase (Fig. 4c) enriched in aluminum and depleted in the base cations respect to the pristine glass of the Colli Albani (Table 1EA). Noteworthy, euhedral zeolite crystals are present in the amorphous, pale yellow phase (Fig. 4c). This textural equilibrium indicates that the zeolites and the amorphous phase formed both at high temperature conditions (up to ~600 °C; e.g. Trolese et al., 2017) during the degassing and cooling of the TVS. Noteworthy, the amorphous, pale yellow phase shows an Al-rich and base cations-poor composition similar those of halloysite crystals (Fig. 5). The K-foiditic glass turned in the amorphous phase is at the origin of the phonotephritic to shoshonitic bulk composition of the TVS bedrock (Fig. 2). Actually, this high-T, sindepositional process removes large part of the base cations from the original K-foiditic matrix and produces a relative increase of silica content in the TVS bedrock (Fig. 2). However, the bulk composition of Colli Albani soils show higher silica content respect those of TVS bedrock (Fig. 2).

4.1.1. Basic properties of the soils

The studied soils range from clayey to sandy, from gray to brown in colour and are characterized by density spanning from 1.01 to 1.35 g/cm^3, neutral pH (6.9 ± 0.8) and low organic matter content (0.70–2.55 wt%; Table 1). The more frequent, dark-to bright-brown soils are generally clay in texture and show lower pH, lower density and higher organic matter content compared to the gray sandy soils. The CEC ranges from medium (~16 cmol (+) kg^{-1}) to high (~25 cmol (+) kg^{-1}). Noteworthy, despite the lower clay and organic matter contents the gray sandy soils show higher CEC compared to the dark to bright-brown clay soils (Table 1).

4.2. Mineralogical composition of soils

Fine-earth fraction of soils show primary (i.e. those occurring in the bedrock) and secondary minerals (i.e. those not occurring in the

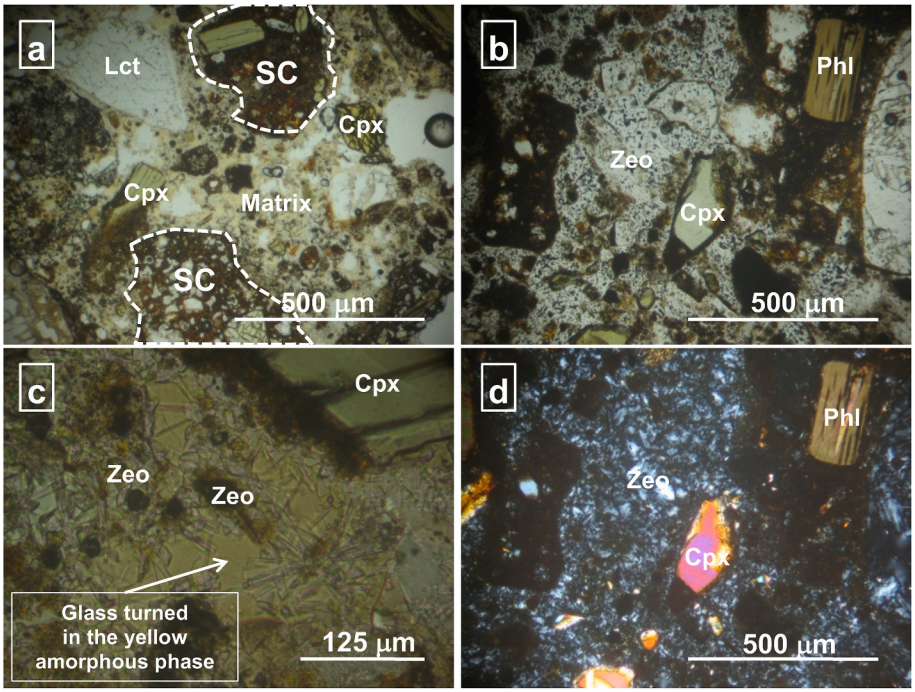

Fig. 4. Photomicrographs of the TVS bedrock in plane-polarized light (a, b, c) and crossed polars (d). Texture of the pyroclastic bedrock made up of porphyric scoria clasts (SC) enclosed within a crystal-rich matrix (photo a). The ash matrix is consolidated and turned into different zeolites (photos b and d) or in pale yellow, glass-like halloysite + zeolites (photo c). Cpx: clinopyroxene; Phl: phlogopite; Lct: leucite; Zeo: zeolites; SC: scoria clast. (For interpretation of the references to colour in this figure legend, the reader is referred to the Web version of this article.)

Table 2
Mineralogical composition of Colli Albani bedrock and soils obtained with XRD.

Sample	Rock/soil type	Lct	Cpx	Phl	Anl	Cbz	Php	Ap	Kfs	Qz	Ab	Hal-7	Sm/mixed layers	Hem
GT8	TVS Bedrock	14	27	18	15	6	18	±	2*					
PA3	Lct-bearing	1	7	42	43	3	1	1	1			1		
PA7		3	15	22	41	4	10		2			3		
PA10		5	21	27	23	3	12		4			4		
PA11		7	15	19	33	3	15	1	2			4		
PA1	Qz-bearing		17	13		1			8	38	3	18	1	1
PA2			6	11					10	39	5	27	1	1
PA4			9	6					8	53	4	17	1	2
PA5			4	9					15	48	3	19	1	1
PA6			22	9		1			16	28	3	22	1	1
PA8			9	9					21	46	2	11	1	1
PA9			8	18					14	35	9	14	1	1
PA12			3	6					10	66	4	9	1	1
PA13			28	27					16	14	3	10	1	1

Lct: leucite; Cpx: clinopyroxene; Phl: phlogopite; Anl: analcime; Cbz: chabazite; Php: phillipsite; Ap: apatite; Kfs: K-feldspar; Qz: quartz.
Ab: albite; Hal-7: halloysite-7Å,; Sm/mixed layers: smectite or mixed layers with expandable layers; Hem: hematite; *: sanidine.

bedrock). Among the primary minerals leucite, analcime, chabazite and phillipsite are observed only in the sandy soils (hereafter Lct-bearing soils); on the other hand, clinopyroxene and phlogopite occur in all analyzed soils (Table 2). Clinopyroxene shows variable shape. Fresh crystals are prismatic while the weathered clinopyroxenes are characterized by a unique "gothic" texture (Fig. 6). The latter is formed by etch pits developed on the crystal cleavage planes. In detail, the walls of pits borders have a variable thickness (up to <1 μm) and can end with conical structures (Fig. 7). The phlogopite in the clay soils shows a worse basal cleavage and higher Fe amount than the phlogopite crystals from the bedrock and sandy soils (Fig. 8). These textural and chemical features are coupled with decreasing of distance between the (001) crystallographic planes. Actually, the XRD peak corresponding to (001) basal planes for the phlogopite moves from 1.01 nm in the bedrock and in the sandy, Lct-bearing soils to 0.99 nm in the clay soils (Table 3EA).

Among the secondary minerals quartz, albite, hematite, and mixed layered clays occur only in the clay soils (hereafter Qz-bearing soils), whereas K-feldspar and halloysite occur in both soil groups (Table 2). Quartz shows elongated/prismatic shape, crystalline faces, clay inclusions and holes (Fig. 9a–c). Hematite is typically botryoidal in texture (Fig. 9d) according to the authigenic origin. SEM images indicate that halloysite is different in the two types of soils. The Lct-bearing soils shows fine grained, globular halloysite (Fig. 3aEA), that occurs as larger, tabular forms in Qz-bearing soils (Fig. 3bEA). A broad XRD peak at about 1.5 nm, in the Qz-bearing soils, suggests the presence of a swelling phase such as discrete smectite or random ordered mixed layered clays with smectite layers.

4.3. Soil chemical composition

According to the occurrence of smectite layers, the Qz-bearing soils show the water loss up to ~100 g/kg (Table 3) at low temperature (≤105 °C) while, the Lct-bearing soils, devoid of mixed layered minerals, have a water loss of ~40 g/kg at T ≤ 105 °C. The total water loss of the Lct-bearing soils in response to heating is lower than that estimated in the Qz-bearing soils (~140 *vs* ~210 g/kg) and concentrated at 105 °C ≤ T ≤ 550 °C. The two groups of soils have higher total water content (Table 1) and lower Ca, Mg, Na, K total contents compared to those

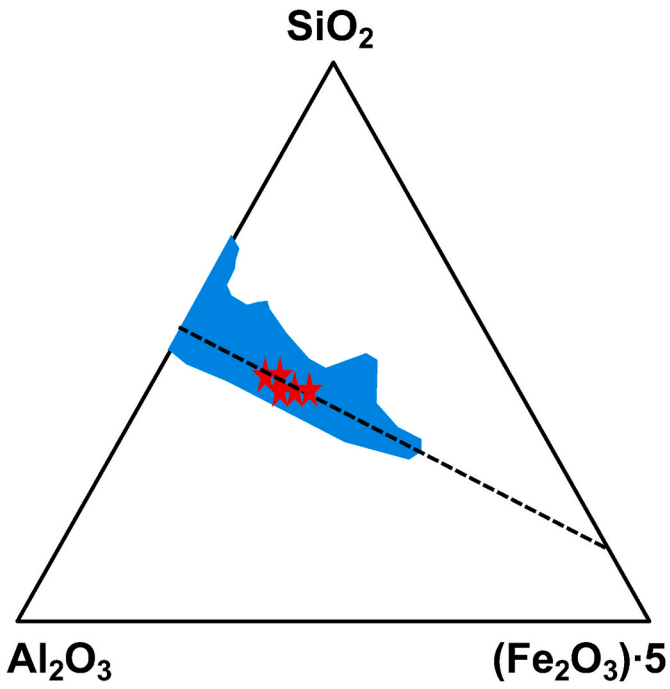

Fig. 5. Chemical composition of the amorphous yellow phase in the TVS bedrock (red stars) reported in the Fe_2O_3*5-Al_2O_3–SiO_2 diagram. The blue field represents the composition of halloysite minerals (data from Joussein et al., 2005). (For interpretation of the references to colour in this figure legend, the reader is referred to the Web version of this article.)

measured in the TVS bedrock (Table 2EA). These chemical features cause an increase of Si, Al and Fe molar fraction (i.e. (Si or Al or Fe)$_{mol}$/Σcations$_{mol}$) of the Lct-bearing and Qz-bearing soils respect to the TVS bedrock (Fig. 10). However, the two groups of soils show a different increase of Si compared to the Al and Fe contents. Actually, the average Si_{Tot}/Al_{Tot} ratio is ~2 in TVS bedrock, Lct-bearing and Qz-bearing soils while, the average Si_{Tot}/Fe_{Tot} ratio is ≈ 4–5 in the TVS bedrock and Lct-bearing soils and ≈2 in the Qz-bearing soils (Table 3). In addition, the decrease of the Ca, Mg, K and Na content is more pronounced in the Qz-bearing soils. Thus, the average $(Ca + Mg + K + Na)_{Tot}/Fe_{Tot}$ ratio in the TVS bedrock, Lct-bearing and Qz-bearing soils is 3, 1 and 0.1, respectively (Table 3). Similar trends are observed for elements leached in the laboratory with deionized water (W subscript) and ammonium acetate (Ex subscript; Table 4). The Si_w/Al_w ratio reflects the soils total composition being ~2 except for two Qz-bearing soils (PA5 and PA12) showing higher ratios (~6–7). The Qz-bearing soils are also characterized by the lowest Fe_w contents (Table 4). However, excluding the Fe_w-poor samples the Qz-bearing and Lct-bearing soils show similar $(Ca + Mg + K + Na)_w/Fe_w$ ratio. Differently, the $(Ca + Mg + K + Na)_{Ex}/Fe_{Ex}$ average ratio is higher in the Lct-bearing than in the Qz-bearing soils (i.e. 775 and 225, respectively).

5. Discussion

The studied soils show textural, mineralogical and chemical differences despite their occurrence in a relatively restricted area characterized by a homogeneous geological substrate made up of the Tufo di Villa Senni pyroclastic flow deposit (Fig. 1). In particular, the bedrock is formed by pyroclastic rocks originated from K-foiditic magmas (Fig. 2) characterized by the high K_2O/SiO_2 ratio and high CaO content. These chemical peculiarities are reflected in the abundance of leucite, clinopyroxene and phlogopite crystals in both bedrock and soils. Clinopyroxene and phlogopite are present in both the Lct-bearing and the Qz-bearing soils confirming the common origin of the two groups of soils. According to the origin from a hot pyroclastic flow deposit, the studied soils show low content of organic matter. Thus, the pH is close to the neutrality and, in turn, the concentrations of active Al and Fe are at the

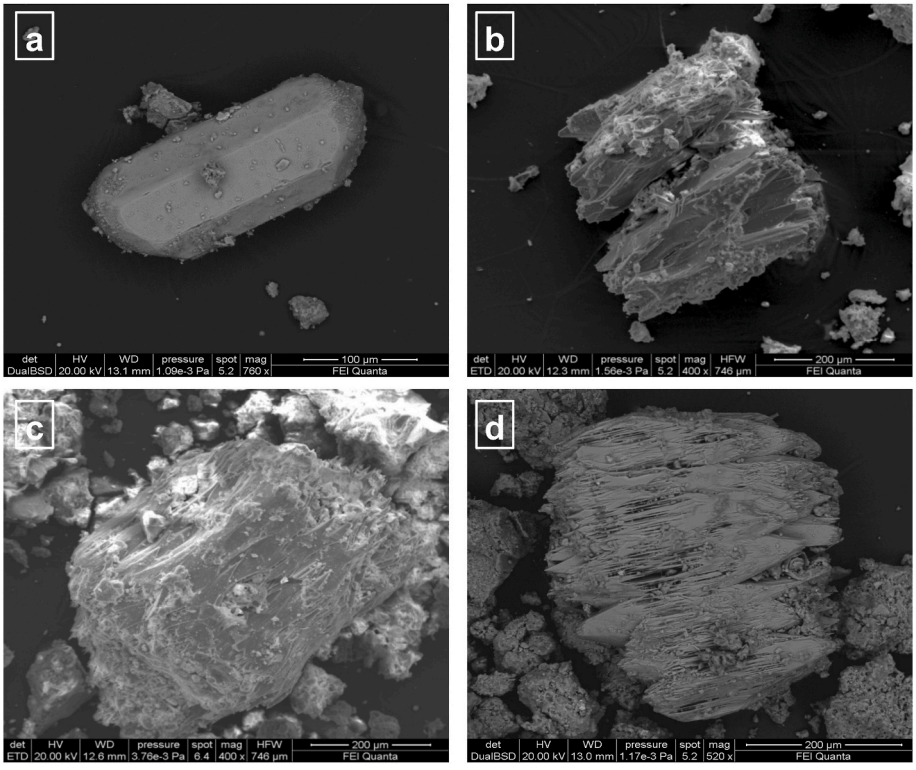

Fig. 6. Secondary electrons (SE) images of clinopyroxenes in the Colli Albani soils. Euhedral crystal of clinopyroxene in the Lct-bearing soil (photo a, sample PA7). Clinopyroxenes with "gothic" texture in the Qz-bearing soils (photos b and c, sample PA13; photo d, sample PA9).

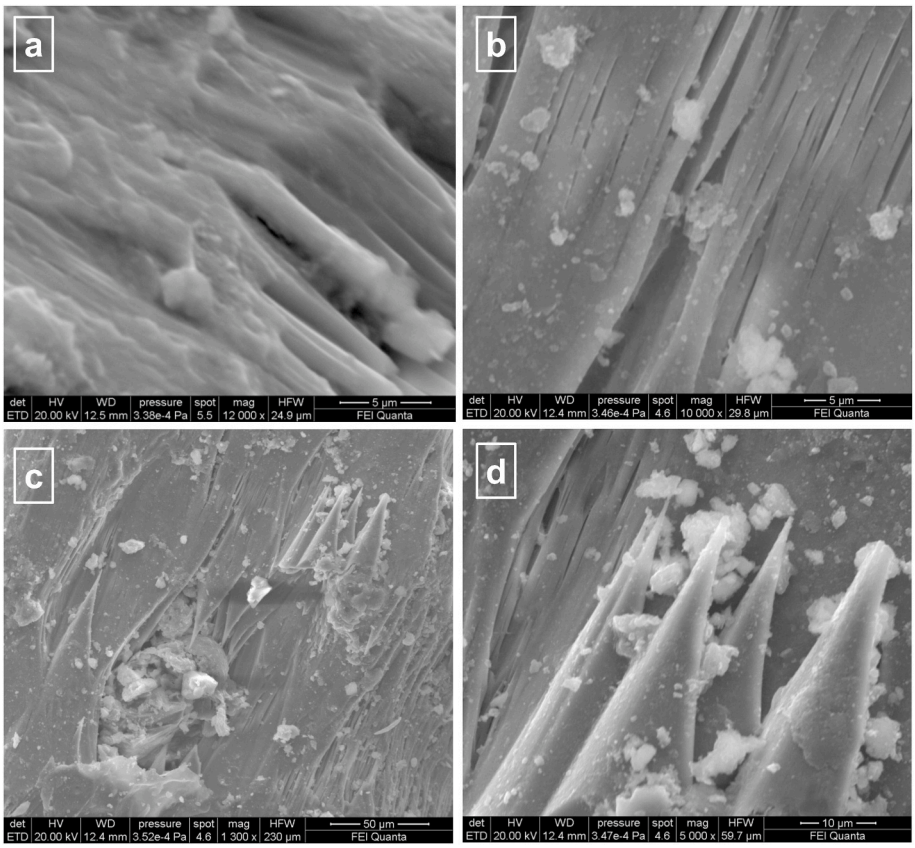

Fig. 7. Details of the "gothic" texture reported in Fig. 5. SE images showing etch pits developed on the crystal cleavage planes (photo a; sample PA4), walls of pits borders (photo b; sample PA13) with variable thickness (up to <1 µm) that can terminate with conical structures (photos c and d; sample PA13).

minimal (Dahlgren et al., 2004). The Lct-bearing soils are weakly weathered volcanic materials, dominated by primary minerals, and comparable to the vitric andosols. However, glass absence, totally independent of the soil-forming processes, makes not appealing the use of vitric term for the soil classification. Glasses are relatively rare in the Colli Albani volcanic rocks because the parental magmas have low viscosity as consequence of their Si -poor and alkali-rich composition (Gaeta et al., 2021). The low viscosity increases, indeed, the crystal growth rate and hampers glass formation in the pyroclastic rocks (e.g. Bonechi et al., 2020). Consequently, the occurrence and/or abundance of glasses cannot be used to discriminate the evolutionary stage of Colli Albani soils. More useful appears the conservation of soft primary minerals (leucite and zeolites) or the quartz presence. In the Qz-bearing soils, quartz is fine grained and, as commonly observed in grains smaller than 100 µm, shows flat plates morphology (e.g. Drees et al., 1989). However, being in almost all the Qz-bearing soils the most abundant mineral (Table 2), quartz is a key mineral to identify pedogenetic processes in studied soils because is totally absent in the bedrock. Actually, the quartz-free, huge pyroclastic-flow deposits of Colli Albani mantle the surface with a volcanic cover spreading radially as far as 50 km from the vent and reaching up to 20 m in thickness, locally. The appearance of quartz in superficial horizons of far soils of the Colli Albani was previously reported by Marra et al. (2009) that excluded an aeolian-origin and attributed the quartz occurrence at the siliciclastic deposits transported by the Tiber River and deposited in the paleo-coastal plane. The area studied in the present work is located inland, far from inferred paleo-coastlines, relatively close to the vent (<10 km) and shows a relatively small, radial hydrographic network that start from the higher point of Colli Albani (Fig. 1). Consequently, surface contamination through colluvial reworking, as well as the bedrock heterogeneity, can be excluded as hypotheses on the quartz origin. The irrelevant aeolian apport in the studied soils is supported by the higher Na_W of the Lct-bearing soils (Table 4 and Fig. 11). Actually, the higher sodium in the soil solution of the higher permeable Lct-bearing soils excludes the buffering effect of sea salt aerosols that interest the Tyrrhenian Sea coast of Latium (Manca et al., 2015). Similarly, the shape of quartz reported in Fig. 9 is entirely convincing of a non-aeolian origin and it is unrealistic, on the other hand, to image that aeolian quartz choses to deposit only in the clayey soils without leucite, and analcime. Therefore, also in absence of independent geochemical data (e.g. $\delta^{18}O$; Wilson 2020), it is realistic to consider the quartz authigenic. The enrichment in the fine-grained clasts, the occurrence of authigenic quartz, swelling minerals and hematite, the decrease of primary minerals, and their location atop the Lct-bearing soils indicate that Qz-bearing soils represent more weathered volcanic material and derive from the Lct-bearing soils. Intriguingly, the Qz-bearing soils show lower CEC respect to the Lct-bearing soils (Table 1). Starting from this framework, the weathering of primary minerals, the neoformation of authigenic minerals and the role of these two groups of minerals in the base cations mobility will be discussed in the following.

5.1. *Weathering of primary minerals*

Clinopyroxene is the main mineral crystallizing in the Colli Albani magmas (e.g. Gaeta et al., 2006). The absence of plagioclase in the Colli Albani rocks (i.e. petrographic peculiarity at global scale) is just one of the evidences of the enlargement of the clinopyroxene stability field in Colli Albani magmas. The absence of plagioclase is caused by the low silica and the high calcium activities that decrease the Gibbs free energy of the diopside solid solution with the $CaFeAlSiO_2$ and $CaAlAlSiO_2$ components. Consequently, the range of the clinopyroxene chemical composition in the Colli Albani rocks is very wide (e.g. SiO_2 = 52-41 wt

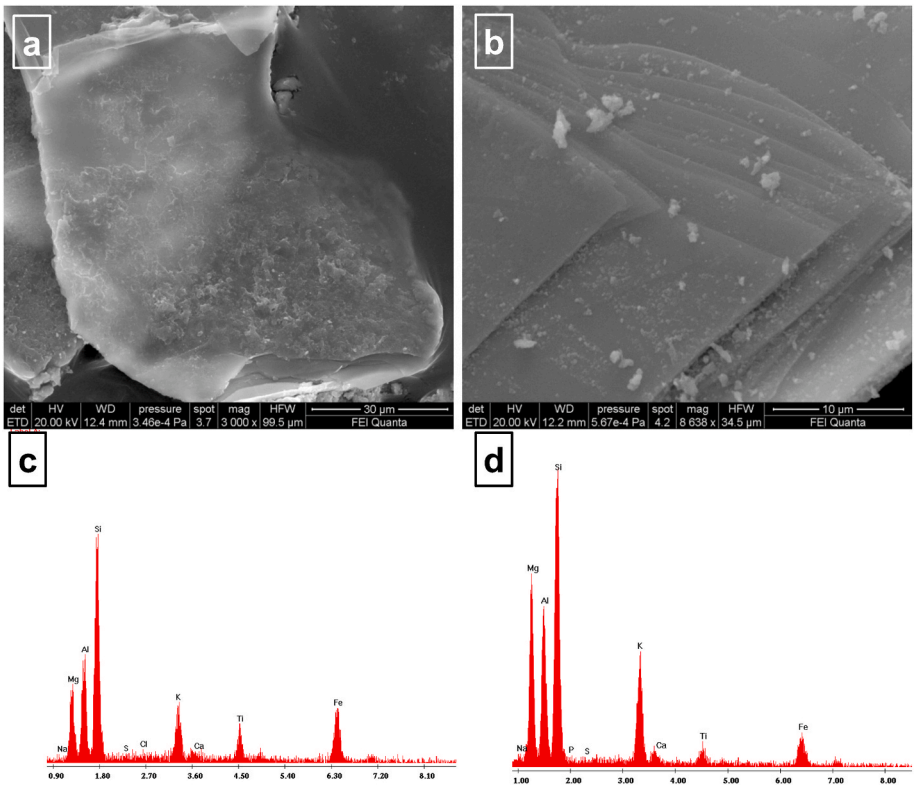

Fig. 8. Secondary electrons images (photos a and b) and energy dispersive spectra (images c and d) of phlogopites in the Lct-bearing (sample PA7) and Qz-bearing (sample PA5) soils. Phlogopite in the Qz-bearing soil (photo a) shows less evident cleavage plane and higher iron amount (image c) than that of the phlogopite in the Lct-bearing soils (photo b and image d).

%; Al_2O_3 = 10-2 wt%; FeO = 15-5 wt%; Gaeta et al., 2021) and this large chemical variation should be taken in account in clinopyroxene dissolution models. Clinopyroxene weathering takes place causing the enlargement and coalescence of etch pits developed on crystal dislocations (Berner et al., 1980). This mechanical process is certainly non-linear in the Colli Albani clinopyroxenes because different, intracrystalline dissolution rates are expected in chemical zoned crystals. The termination of the conical morphologies (Fig. 7d) shows Si enriched composition (Fig. 4EA) suggesting that these are the clinopyroxene zones with lower dissolution rate, probably because are also Fe-poor (e.g. Monasterio-Guillot et al., 2021). The coalescence of zones at different dissolution rates, caused by the large chemical variation of the single crystal, is at the origin of the "gothic" texture that characterizes the weathered clinopyroxenes in the Colli Albani soils (Figs. 6 and 7). The positive correlation between Ca_W and Mg_W contents (Fig. 11a) indicates that the weathered clinopyroxene releases Ca and Mg in the water circulating in the soils. The Qz-bearing soils, which are characterized by lower Ca and Mg total contents than the Lct-bearing soils, show higher Ca_W and Mg_W contents according to a more intense stage of weathering of clinopyroxene (Fig. 7). Moreover, the Mg_W/Ca_W atomic ratio <1 indicates that Fe is released from the weathered clinopyroxene together Mg. Clinopyroxene and phlogopite in the bedrock are, indeed, abundant and relatively Fe-rich (FeO_{Tot} up to ~12 wt%; Table 1EA) and their contribution to the Fe enrichment in soils is certainly higher than that of Ti-magnetite, whose abundance is low in the bedrock (<1 vol%). The phlogopite in the Qz-bearing soils has a lower basal spacing than that observed for the phlogopite occurring in both Lct-bearing soils and TVS bedrock (Table 3EA). The decrease of the basal spacing in the phlogopite cannot be explained by the replacement of K with hydrated exchangeable cations. This process, indeed, should lead to an increase in the phlogopite basal spacing. Nevertheless, the relatively high K_{Ex} content in the Qz-bearing soils (Table 4) is certainly due to the phlogopite leaching as leucite, analcime and other zeolites are absent/scarce and the alkali feldspars appear stable as indicated by their abundance (Table 2) and the absence of the K_W *vs* Na_W correlation (Fig. 11b). The increase of Fe in the phlogopite (Fig. 8) and the $K_{Ex} + Mg_{Ex}$ *vs* Fe_{Ex} correlation observed in the Qz-bearing soils (Fig. 12) indicate that that the shortening of the interlayer distance along the c-axis is caused by the Fe-oxy substitution reaction:

$$K^+ + Mg^{2+} + 3(OH)^- \rightleftharpoons Fe^{3+} + 3O^{2-} + 3H^+.$$

The K_W *vs* Na_W opposite trends of the two groups of soils (Fig. 11b) suggest that the phlogopite weathering occur by a different process with respect to the leucite, analcime and other zeolites. As discussed above, the early stage of weathering for phlogopite and clinopyroxene affects the cleavage planes where the surface protonation and deprotonation it is favored. Thus, surface reactions are the rate-limiting of the clinopyroxene and phlogopite weathering. Due to their highly polymerized structures, leucite, analcime and other zeolites lack of preferential cleavage planes that favor protonation. The leucite to analcime conversion is a fast reaction (i.e. a few days at temperatures between 150 and 300 °C) with a low activation energy (Gupta and Fyfe 1975; Putnis et al., 2007). On the other hand, analcime is highly soluble at 25 °C (Wilkin and Barnes, 1998). Therefore, leucite and analcime and, in general, zeolites, can be considered readily soluble minerals. The chemical alteration of highly soluble minerals is limited by the dissolving components' rate can be transported away from the mineral-water interface. The large sandy fraction (Table 1) of the Lct-bearing soils supports leaching conditions in which leucite, analcime and zeolites are quickly dissolved.

5.2. *Authigenic mineral formation*

Halloysite is the most common clay minerals in the studied soils (Fig. 3EA and Table 2) because its formation is favored by the Al-rich, base

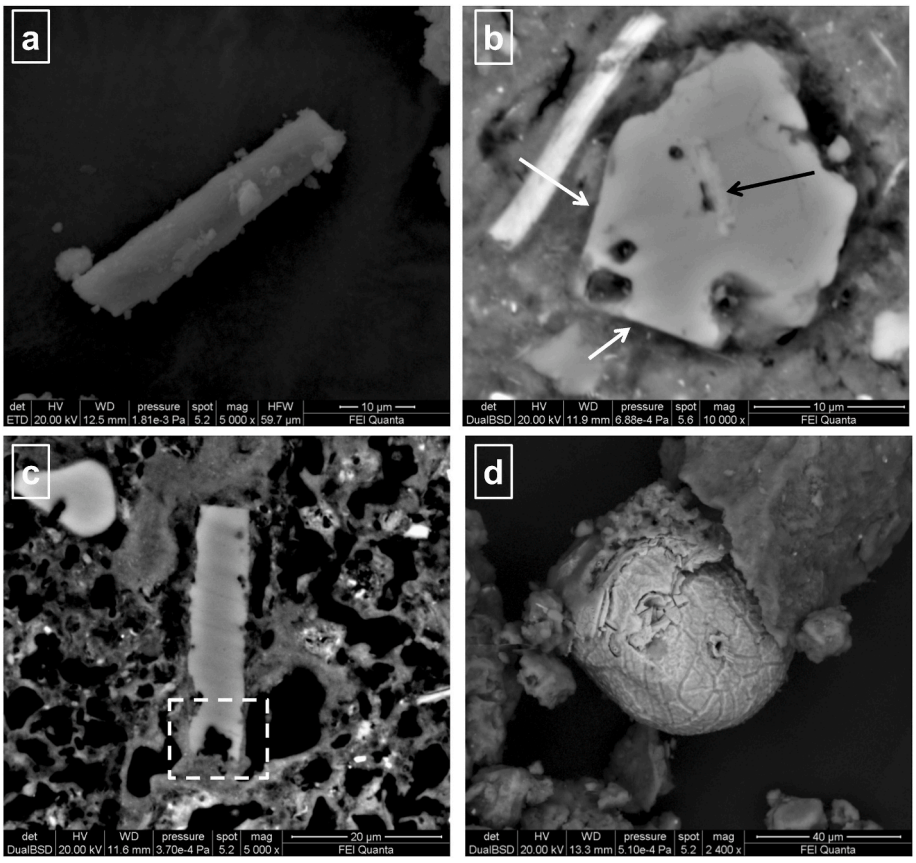

Fig. 9. Secondary electrons images of quartz and hematite in the Qz-bearing soils. The photos show: elongated quartz in sample PA13 (a); quartz with crystalline faces (withe arrows) and inclusion of halloysite (black arrow) in sample PA1(b); elongated quartz growing on the soil pore (white rectangle) in sample PA13 (c) and botryoidal hematite in sample PA2 (d).

Table 3
Selected total content ratios and water loss at various temperature (g kg^{-1}).

Sample	Rock/soil type	Si_{Tot}/Al_{Tot}	Si_{Tot}/Fe_{Tot}	$(Ca + Mg + K + Na)_{Tot}/Fe_{Tot}$	105 °C	550 °C	950 °C
GT8	TVS bedrock	2.3	4.2	2.6	18.5	44.6	7.0
PA3	Lct-bearing	2.5	5.9	1.3	37.3	89.8	8.8
PA7		2.2	4.7	0.7	38.6	93.3	4.6
PA10		1.7	3.5	0.7	42.5	90.8	10.8
PA11		1.8	4.2	1.0	29.0	87.4	9.2
PA1	Qz-bearing	2.0	2.7	0.1	41.4	113.8	11.4
PA2		1.5	1.8	0.1	90.6	128.2	10.8
PA4		2.0	2.4	0.2	52.2	121.8	14.1
PA5		1.4	1.9	0.1	75.3	137.3	8.0
PA6		2.1	2.4	0.1	75.0	122.7	9.8
PA8		1.8	2.5	0.2	87.0	126.1	8.3
PA9		1.6	2.2	0.1	100.2	109.8	14.6
PA12		1.6	2.5	0.1	76.6	114.0	12.5
PA13		1.6	2.7	0.1	98.5	111.5	11.8

cations-poor composition of the amorphous phase in the TVS bedrock (Fig. 4). This halloysite-like composition (Fig. 5) develops during the degassing of the pyroclastic flow deposit at high temperatures (up to ~600 °C; e.g. Trolese et al., 2017). In particular, the pristine K-foiditic glass has been hydrated and leached of all major mobile elements except Al (Table 1EA; Fig. 2). Such Al-enrichment favors the incipient crystallization of fine grained halloysite with globular morphology in the Lct-bearing soils (Fig. 3aEA). By the progressive weathering of the Colli Albani pyroclastic rocks, the halloysite stability field increases and the larger, tabular halloysite crystals may form in the Qz-bearing soils (Fig.3bEA). The water loss up to ~10 wt% at low temperature (≤105 °C) in the Qz-bearing soils (Table 3) also indicates the presence of other hydrates silicates (smectites and/or mixed layers with expandable layers) beside halloysite. Such a kind of mixed layering has been observed in similar phlogopite-bearing deposits affected by chemical alteration in karst environment (Aldega et al., 2009). The formation of discrete smectite (S) or smectite layers interlayered with phlogopite is favored by the increase of Mg and Ca activities in the soil water, which, in turn, result controlled by the chemical alteration of the clinopyroxene in the Qz-bearing soils. The symmetric (001) peak of halloysite (H) seems exclude the formation of H–S mixed-layered clays (Ranst et al., 2020, Fig. 5EA). The mixed layered clays are, however, scarce because also in the Qz-bearing soils there are leaching conditions that favor the halloysite formation. Due to the low amount of organic matter, the leaching at neutral pH conditions, also promotes the Fe fixation as oxy-phlogopite and hematite (Fig. 9d) and lead to the increase of the

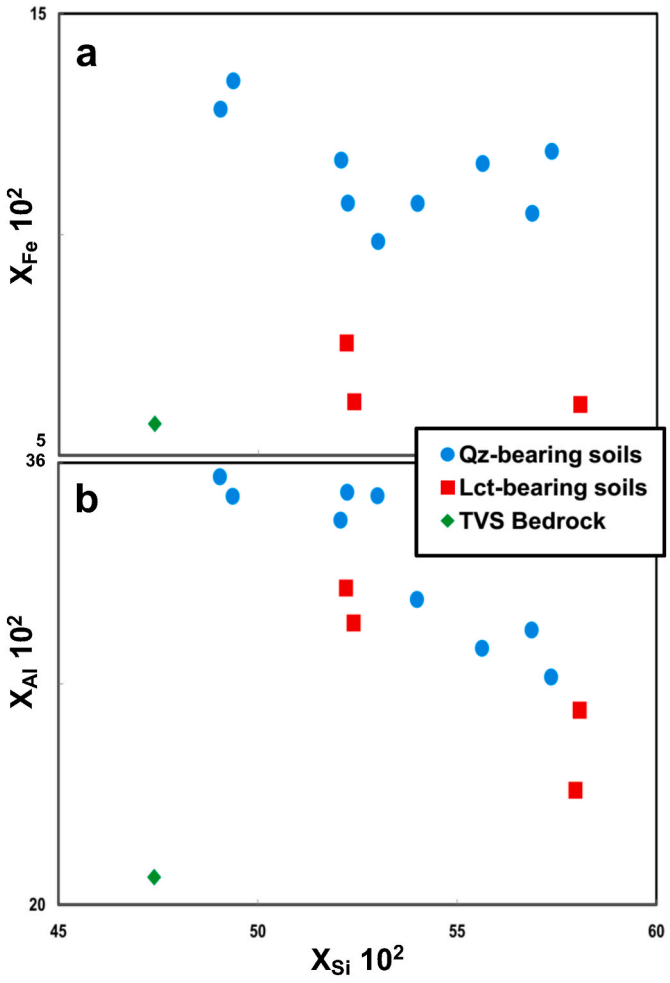

Fig. 10. Total Si, Al and Fe contents of the TVS bedrock, Lct-bearing and Qz-bearing soils reported as molar fraction (i.e. (Si or Al or Fe)$_{mol}$/ Σcations$_{mol}$*10^2).

silica activity (Fig. 10) that is supported by the neoformation of quartz and alkali feldspar (Table 2). In fact, the elongated shape, the crystalline faces, the halloysite inclusions and the holes (Fig. 9a–c) indicate an authigenic origin of quartz occurring in the Qz-bearing soils.

5.3. Role of primary minerals in the base cations mobility

The Qz-bearing soils are characterized by low amounts of exchangeable K and Na compared to the Lct-bearing soils. The average Alkali$_{Ex}$/Alkali$_{Tot}$ ratio of the two groups of soils is similar (~0.08) and the main alkali-bearing minerals occurring in the Qz-bearing soils are the phlogopite and the authigenic alkali feldspar. Consequently, the decrease of exchangeable K and Na in the Qz-bearing soils is due to the decrease of total amount and the speciation of the alkali-bearing minerals. Phlogopite crystals appear relatively resistant to the chemical alteration throughout the Fe-oxy reaction that releases K and Mg and immobilizes the Fe (Fig. 12). Thus, the absence of leucite, analcime and zeolites indicates that the phlogopite (±authigenic alkali feldspar) is the main source for K_{Ex} in the Qz-bearing soils. On the other hand, the higher amount of the K_{Ex} and Na_{Ex} measured in the Lct-bearing soils depends on the presence of highly soluble leucite and zeolites (Table 4). However, in leaching conditions the contribution of leucite, analcime and zeolites to the base cations mobility should be considered a process

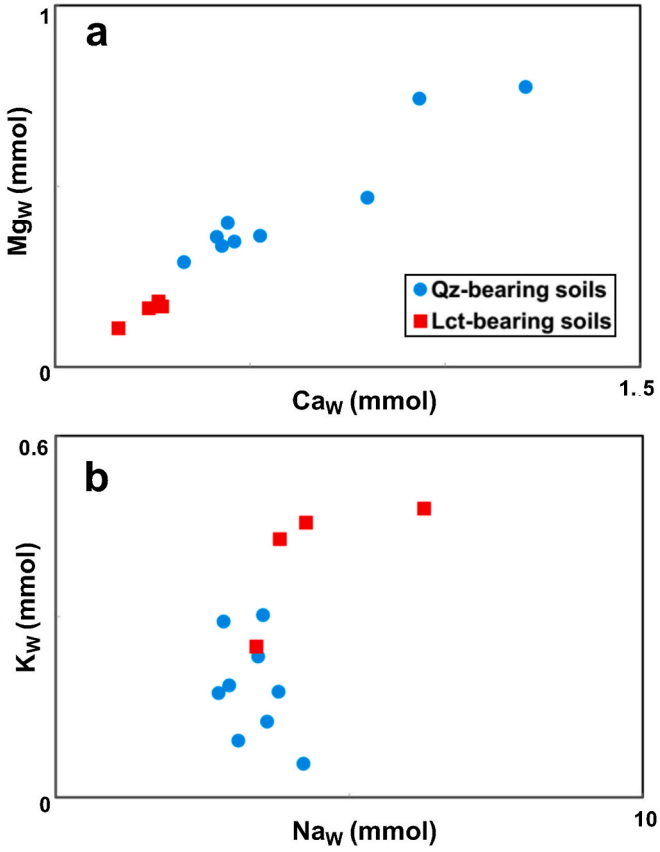

Fig. 11. Ca_W, Mg_W, K_W and Na_W contents of the Lct-bearing and Qz-bearing soils. The two groups of soils show positive correlation between Ca_W and Mg_W contents (diagram a), while K_W and Na_W abundances form opposite trends (diagram b).

Table 4
Cations (mg kg^{-1}) extracted from soils using deionized water (cation$_W$) and ammonium acetate (cation$_{Ex}$).

Sample	Soils type	Si_W	Al_W	Fe_W	Mg_W	Ca_W	Na_W	K_W	Fe_{Ex}	Mg_{Ex}	Ca_{Ex}	Na_{Ex}	K_{Ex}
PA3	Lct-bearing	263	116	36	3	6	79	10	8	640	2200	600	1200
PA7		314	134	42	4	11	144	19	5	340	1900	1359	2678
PA10		326	173	58	4	11	98	18	7	433	2207	1013	1847
PA11		299	145	48	4	10	88	17	8	320	2520	1081	1662
PA1	Qz-bearing	256	143	59	11	32	66	11	19	460	2080	122	340
PA2		240	110	43	9	17	83	5	13	420	1900	1040	700
PA4		207	117	51	18	37	81	12	11	520	2450	580	802
PA5		73	11	4	19	48	68	7	17	700	1900	83	129
PA6		196	88	35	8	18	64	7	21	560	2140	108	117
PA8		307	179	64	9	21	79	9	17	700	2120	80	129
PA9		428	244	91	10	18	87	7	11	780	2240	421	219
PA12		195	28	11	7	13	97	2	19	760	1960	221	117
PA13		251	110	44	8	17	71	4	17	580	2220	78	199

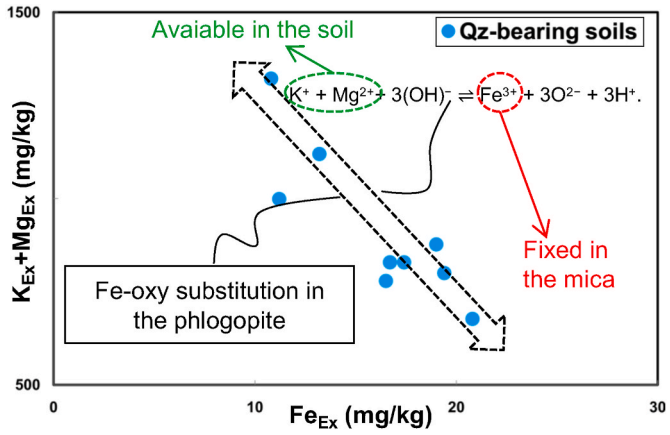

Fig. 12. Abundance of the potassium, magnesium and iron obtained from the Qz-bearing soils leached with the ammonium acetate. The correlation between K_{Ex} + Mg_{Ex} and Fe_{Ex} in the Qz-bearing soils supports the Fe-oxy substitution reaction in the phlogopite (see text) that releases magnesium and potassium in the soils and fixes the iron in the mica.

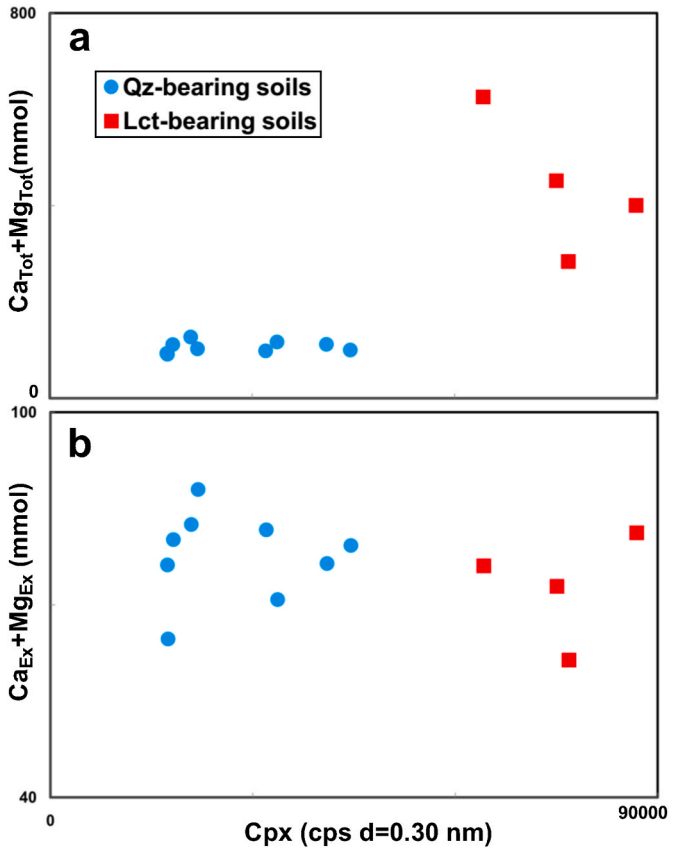

Fig. 13. Ca_{Ex}, Mg_{Ex}, Ca_{Tot} and Mg_{Tot} contents of the Lct-bearing and Qz-bearing soils. Cation contents are plotted versus the abundance of clinopyroxene expressed as counts per second (CPS) of the X ray diffraction peak at d = 0.30 nm.

of bulk solubility. A process mediated by the specific surface controls the release of Mg and Ca from the clinopyroxene. The Mg and Ca total contents are higher in the Lct-bearing than in the Qz.-bearing soils, in agreement with the clinopyroxene abundance estimated for the two groups of soils (Fig. 13a). Differently, the Mg_{Ex} and Ca_{Ex} (Fig. 13b) and the Mg_W and Ca_W contents (Fig. 11a) measured in the Qz-bearing soils are respectively similar and higher than those measured in the Lct-bearing soils. The data on the Mg and Ca leached in the laboratory indicate the presence of a large number of sites where Mg and Ca can be removed despite the lower clinopyroxene abundance in the Qz-bearing soils. Actually, the "gothic texture" (Figs. 6 and 7) of the deeply weathered clinopyroxenes allows for an increase in the active surface where Mg and Ca can be released in the Qz-bearing soils.

6. Conclusions

The Colli Albani soils developed on low silica, high alkali and high CaO pyroclastic flow deposits that were emplaced at high temperature. The peculiar chemical composition of such deposits and the high temperature are responsible for three features that have influenced deeply the soil-forming processes in the Colli Albani: i) the scarcity of glass; ii) the presence of a halloysite-like amorphous phase and ii) the low content of organic matter. Consequently, Colli Albani soils are typically glass-free already in the incipient weathering stage, always halloysite-bearing and neutral pH. The presence of highly soluble leucite and analcime or the occurrence of authigenic quartz allow us to define an evolutionary stage of soil development for the Colli Albani. Leucite-bearing soils constitute weakly weathered volcanic material formed at an early stage of chemical alteration where incipient halloysite crystallization with globular shape takes place. On the other hand, quartz-bearing soils developed after an intense stage of chemical alteration where phlogopite and clinopyroxene are the only preserved primary minerals. In such soils, phlogopite and clinopyroxene are associated with abundant tabular-shape halloysite and quartz, alkali feldspar, hematite, and smectites. Leucite-bearing soils, in which abundant K and Na are released from the highly soluble leucite and zeolites, show a higher CEC than that observed for the quartz-bearing soils. However, the CEC of quartz-bearing soils is rarely <20 cmol (+) kg^{-1} for the buffer effect of the oxy-reaction affecting the phlogopite, that releases K + Mg and immobilizes the Fe. Furthermore, the strongly weathered clinopyroxenes with the "gothic texture", enhance the release Ca and Mg in the soil. Current base cations fertilization recommendations are based on the amount of water-soluble or exchangeable base cations. Data on the Colli Albani soils suggest that the limit between these two nutrients is almost vague in the case of leucite, analcime, clinopyroxene and phlogopite. Actually, the CEC values, reported in almost the totally of the chemical reports on the Colli Albani soils, include base cations not deriving from minerals with exchanging properties. Consequently, an effort to define the processes that govern the extraction of the base cations from leucite, analcime, clinopyroxene and phlogopite will be desirable.

Declaration of competing interest

The authors declare that they have no known competing financial interests or personal relationships that could have appeared to influence the work reported in this paper.

Data availability

Data will be made available on request.

Acknowledgment

This research was partially founded by Sapienza Ateneo 2019 medi/Gaeta. We thank T. Ruspandini (Sapienza, Università di Roma) and M. Serracino (CNR-IGAG) for assistance during SEM and EPMA analytical sessions and I. Palermo for drawing some figures.

Appendix A. Supplementary data

Supplementary data to this article can be found online at https://doi.org/10.1016/j.apgeochem.2022.105430.

References

Aldega, L., Cuadros, J., Laurora, A., Rossi, A., 2009. Weathering of phlogopite to beidellite in a karstic environment. Am. J. Sci. 309, 689–710. https://doi.org/10.2475/08.2009.03.

Astolfi, M.L., Di Filippo, P., Gentili, A., Canepari, S., 2017. Semiautomatic sequential extraction of polycyclic aromatic hydrocarbons and elemental bio-accessible fraction by accelerated solvent extraction on a single particulate matter sample. Talanta 174, 838–844. https://doi.org/10.1016/j.talanta.2017.06.072.

Astolfi, M.L., Protano, C., Marconi, E., Massimi, L., Brunori, M., Piamonti, D., Migliara, G., Vitali, M., Canepari, S., 2020. A new treatment of human hair for elemental determination by inductively coupled mass spectrometry. Anal. Methods 12, 1906–1918. https://doi.org/10.1039/C9AY01871A.

Berner, R.A., Sjöberg, E.L., Velbel, M.A., Krom, M.D., 1980. Dissolution of pyroxenes and amphiboles during weathering. Science 207 (4436), 1205–1206. https://doi.org/10.1126/science.207.4436.1205.

Bonechi, B., Perinelli, C., Gaeta, M., 2020. Clinopyroxene growth rates at high pressure: constraints on magma recharge of the deep reservoir of the Campi Flegrei Volcanic District (south Italy). Bull. Volcanol. 82, 5. https://doi.org/10.1007/s00445-019-1342-5.

Bozzano, F., Gaeta, M., Marcoccia, S., 2006. Weathering of valle ricca stiff and jointed clay eng. Geol. 84, 161–182. https://doi.org/10.1016/j.enggeo.2005.11.010.

Dahlgren, R.A., Saigusa, M., Ugolini, F.C., 2004. The nature, properties and management of volcanic soils. Adv. Agron. 82, 113–182.

Drees, L.R., Wilding, L., Smeck, N.E., Senkayi, A.L., 1989. Silica in Soils: Quartz and Disordered Silica Polymorphs. Minerals in Soil Environments, second ed. Soil Science Society of America, Madison, Wisconsin, USA. https://doi.org/10.2136/sssabookser1.2ed.c19. 313–974.

Fabbrizio, A., Gaeta, M., Carroll, M.R., Petrelli, M., 2018. Crystallization induced Sulfur and REE zoning in apatite: the example of the Colli Albani's magmatic system. Eur. J. Mineral 30, 125–133. https://doi.org/10.1127/ejm/2018/0030-2701.

Freda, C., Gaeta, M., Palladino, D.M., Trigila, R., 1997. The Villa Senni Eruption (Alban Hills, central Italy): the role of H_2O and CO_2 on the magma chamber evolution and on the eruptive scenario. J. Volcanol. Geoth. Res. 78, 103–120. https://doi.org/10.1016/S0377-0273(97)00007-3.

Freda, C., Gaeta, M., Giaccio, B., Marra, F., Palladino, D.M., Scarlato, P., Sottili, G., 2011. CO_2-driven large mafic explosive eruptions: the Pozzolane Rosse case study from the Colli Albani Volcanic District (Italy). Bull. Volcanol. 73, 241–256. https://doi.org/10.1007/s00445-010-0406-3.

Gaeta, M., 1998. Petrogenetic implications of Ba-sanidine in the lionato tuff (Colli Albani volcanic district, Central Italy). Mineral. Mag. 62, 697–701. https://doi.org/10.1180/002646198547927.

Gaeta, M., Fabrizio, G., Cavarretta, G., 2000. F-phlogopites in the Alban Hills Volcanic District (Central Italy): indications regarding the role of volatiles in magmatic crystallisation. J. Volcanol. Geoth. Res. 99, 179–193. https://doi.org/10.1016/S0377-0273(00)00172-4.

Gaeta, M., Freda, C., Christensen, J.N., Dallai, L., Marra, F., Karner, D.B., Scarlato, P., 2006. Time-dependent geochemistry of clinopyroxene from the Alban Hills (Central Italy): clues to the source and evolution of ultrapotassic magmas. Lithos 86, 330–346. https://doi.org/10.1016/j.lithos.2005.05.010.

Gaeta, M., Freda, C., Marra, F., Arienzo, I., Gozzi, F., Jicha, B., Di Rocco, T., 2016. Paleozoic metasomatism at the origin of Mediterranean ultrapotassic magmas: constraints from time-dependent geochemistry of Colli Albani volcanic products (Central Italy). Lithos 244, 151–164. https://doi.org/10.1016/j.lithos.2015.11.034.

Gaeta, M., Bonechi, B., Marra, F., Perinelli, C., 2021. Uncommon K-foiditic magmas: the case study of Tufo del Palatino (Colli Albani Volcanic District, Italy). Lithos 396–397, 106239. https://doi.org/10.1016/j.lithos.2021.106239.

Gupta, A.K., Fyfe, W.S., 1975. Leucite survival: the alteration to analcime. Can. Mineral. 13, 361–363.

Joussein, E., Petit, S., Churchman, J., Theng, B., Righi, D., Delvaux, B., 2005. Halloysite clay minerals-a review. Clay Miner. 40, 383–426. https://doi.org/10.1180/0009855054040180.

Kirkman, J.H., Mc Hardy, W.J., 1980. A comparative study of the morphology, chemical composition and weathering of rhyolitic and andesitic glass. Clay Miner. 15, 165–173. https://doi.org/10.1180/claymin.1980.015.2.07.

Manca, F., Capelli, G., Tuccimei, P., 2015. Sea salt aerosol groundwater salinization in the Litorale Romano natural reserve (Rome, Central Italy). Environ. Earth Sci. 73, 4179–4190. https://doi.org/10.1007/s12665-014-3704-9.

Marra, F., Gaeta, M., Jicha, B.R., Nicosia, C., Tolomei, C., Ceruleo, P., Florindo, F., Gatta, M., La, Rosa, M., Rolfo, M.F., 2019. MIS 9 to MIS 5 terraces along the Tyrrhenian Sea coast of Latium (central Italy): assessing interplay between sea level oscillations and tectonic movements. Geomorphology 346, 106843. https://doi.org/10.1016/j.geomorph.2019.106843.

Marra, F., Karner, D.B., Freda, C., Gaeta, M., Renne, P., 2009. Large mafic eruptions at alban hills volcanic district (Central Italy): chronostratigraphy, petrography and eruptive behavior. J. Volcanol. Geoth. Res. 179, 217–232. https://doi.org/10.1016/j.jvolgeores.2008.11.009.

Marra, F., Deocampo, D., Jackson, M.D., Ventura, G., 2011. The Alban Hills and Monti Sabatini volcanic products used in ancient Roman masonry (Italy): an integrated stratigraphic, archaeological, environmental and geochemical approach. Earth Sci. Rev. 108, 115–136. https://doi.org/10.1016/j.earscirev.2011.06.005.

Monasterio-Guillot, L., Rodriguez-Navarro, C., Ruiz-Agudo, E., 2021. Kinetics and mechanisms of acid-pH weathering of pyroxenes. G-cubed 22 (11), e2021GC009711. https://doi.org/10.1029/2021GC009711.

Moore, D.M., Reynolds Jr., R.C., 1997. X-Ray Diffraction and the Identification and Analysis of Clay Minerals. Oxford University Press, Oxford, UK, p. 378. https://doi.org/10.1017/S0016756898501501.

Napoli, R., Paolanti, M., Rivieccio, R., Di Ferdinando, S., 2019. Carta dei suoli del Lazio scala 1:250000. S.E.L.C.A. Firenze.

Putnis, C.V., Geisler, T., Schmid-Beurmann, P., Stephan, T., Giampaolo, C., 2007. An experimental study of the replacement of leucite by analcime. Am. Mineral. 92, 19–26. https://doi.org/10.2138/am.2007.2249.

Ranst, Van, E., Kips, P., Mbogoni, J., Mees, F., Dumon, M., Delvaux, B., 2020. Halloysite-smectite mixed-layered clay in fluvio-volcanic soils at the southern foot of Mount Kilimanjaro, Tanzania. Geoderma 375, 114527. https://doi.org/10.1016/j.geoderma.2020.114527.

Ross, D.S., Ketterings, Q., 1995. Recommended methods for determining soil cation exchange capacity. Recommended soil testing procedures for the northeastern United States 493, 62.

Ruxton, B.P., 1988. Towards a weathering model of mount lamington ash, Papua New Guinea. Earth Sci. Rev. 25, 387–397. https://doi.org/10.1016/0012-8252(88)90006-2.

Shoji, S., Nanzyo, M., Shirato, Y., Ito, T., 1993. Chemical kinetics of weathering in young Andisols from northeastern Japan using 108C-normalized soil age. Soil Sci. 155, 53–60.

Trolese, M., Giordano, G., Cifelli, F., Winkler, A., Mattei, M., 2017. Forced transport of thermal energy in magmatic and phreatomagmatic large volume ignimbrites: paleomagnetic evidence from the Colli Albani volcano, Italy. Earth Planet Sci. Lett. 478, 179. https://doi.org/10.1016/j.epsl.2017.09.004, 19.

Wilkin, R.T., Barnes, H.L., 1998. Solubility and stability of zeolites in aqueous solution: I. Analcime, Na-, and K-clinoptilolite. Am. Mineral. 83, 746–761. https://doi.org/10.2138/am-1998-7-807.

Wilson, M.J., 2020. Dissolution and formation of quartz in soil environments: a review. Soil Sci. Annu. 71, 3–14. https://doi.org/10.37501/soilsa/122398.